Chaos, Solitons and Fractals 42 (2009) 472–482

Contents lists available at ScienceDirect

Chaos, Solitons and Fractals

journal homepage: www.elsevier.com/locate/chaos

Fractal structure in the color distribution of natural images

François Chapeau-Blondeau *, Julien Chauveau, David Rousseau, Paul Richard

Laboratoire d'Ingénierie des Systèmes Automatisés (LISA), Université d'Angers, 62 Avenue Notre Dame du Lac, 49000 Angers, France

ARTICLE INFO

Article history:
Accepted 14 January 2009

ABSTRACT

The colorimetric organization of RGB color images is investigated through the computation of the correlation integral of their three-dimensional histogram. For natural color images, as a common behavior, the correlation integral is found to follow a power law, with a non-integer exponent characteristic of a given image. This behavior identifies a fractal or multiscale self-similar distribution of the colors contained in typical natural images. This finding of a possible fractal structure in the colorimetric organization of natural images complement other fractal properties previously observed in their spatial organization. Such fractal colorimetric properties may be helpful to the characterization and modeling of natural images, and may contribute to progress in vision.

1. Introduction

An important task for image processing is to identify regularities of properties in given classes of images. This is a useful step to characterize images and to elaborate models for them. In turn, efficient image characterization and modeling is helpful to many areas of image processing, image coding, pattern recognition. Also, efficient image characterization and modeling can contribute to the understanding of the visual system and to progress in computer vision.

An important regularity of properties observed for many types of natural images lies in their multiscale or scaling, or fractal, behavior. Natural images tend to display a self-similar spatial organization. This is conveyed by a frequency spectrum exhibiting power-law evolution of the type $1/f^{\alpha}$ with f the spatial frequency [1–4]. Equivalently, power-law evolution of the spectrum is associated with power-law evolution for the spatial correlation function [4]. This type of spatial scaling has been related to structures and details existing at all spatial scales in natural scenes, with objects of many sizes, edges and occlusion, appearing over a wide range of depths or magnifications [5,4,6]. In addition, it has been shown that scaling or multiscale properties are also present in the temporal structure of natural time-varying images. The temporal dynamics of natural images, as captured by vision, exhibit power-law evolution of the spectrum with the temporal frequency [7]. Objects of many sizes, occurring at many depths, will move with many (angular) velocities relative to the observer, conferring scale-invariant spatiotemporal structures to natural images. These findings manifest that natural images do not change in random unstructured ways over space or time. On the contrary, images at different times and spatial positions display correlations, structures, redundancy. And these correlations appear to be self-similar, or scale-invariant, or fractal, over space and time. These recent findings have proved useful to characterize the statistical properties of natural images, but also to shed new light on the coding and processing by the visual system [8,5,9,10]. These findings also represent helpful guidelines to progress in the on-going task of developing models for natural images [11–15].

* Corresponding author.
E-mail address: chapeau@univ-angers.fr (F. Chapeau-Blondeau).

0960-0779/$ - see front matter © 2009 Elsevier Ltd. All rights reserved.
doi:10.1016/j.chaos.2009.01.008

In the present paper, beyond their spatial and temporal aspects, we will examine another aspect of natural images, namely their colorimetric organization. For natural color images, we will use an histogram representation in the colorimetric space in order to enumerate the colors that are present in an image and the frequency (the number of pixels) with which they are represented. This will allow us to establish that, in the colorimetric domain, natural color images also tend to exhibit a nontrivial self-similar, or scale-invariant, or fractal organization, which is distinct from, but possibly related to, its fractal spatial and temporal organizations. Other studies have appeared to characterize the colorimetric statistics of natural images [16], especially to confirm the scale-invariant spatial organization of these images over various chromatic conditions [1,17,18]. However, a statistical characterization establishing a fractal colorimetric organization of natural images as performed here is new to our knowledge. This approach may be specially relevant to contribute to the modeling of color images and the related applications [19–25].

2. Method of fractal characterization

We consider RGB color images, with each component varying among Q possible values at each pixel of spatial coordinate (x_1, x_2). The red component R is denoted $X_1(x_1, x_2)$, the green component G is $X_2(x_1, x_2)$, and the blue component B is $X_3(x_1, x_2)$, all three assuming integer values in $[0, Q-1]$. The histogram of such color images is a three-dimensional structure comprising Q^3 colorimetric cells defined over the cube $[0, Q-1]^3$ in the RGB space. Each pixel (numbered by the index n) of the color image maps into a point P_n in the RGB space which falls in a definite colorimetric cell of the $[0, Q-1]^3$ cube. The number of points falling in each colorimetric cell counts the number of pixels having this color in the image. For the RGB color image, the data structure with the points P_n distributed among the colorimetric cells forms the three-dimensional histogram we will be considering here. For the very common choice $Q = 2^8 = 256$, the histogram with its $2^{24} \approx 16.8 \times 10^6$ colorimetric cells is a large data structure which can display complex organization (see Fig. 7 for example). We are going to show that for natural color images, the three-dimensional histogram tends to display a fractal organization, with structures and details spanning many scales across the colorimetric space.

The characterization of a fractal structure in the colorimetric space will be based here on the computation of a quantity known in fractal studies as the correlation integral [26,27]. From the three-dimensional histogram of a color image, it can be computed as follows. In the colorimetric RGB space, for a given radius r, each point P_n of the three-dimensional histogram is successively taken as the center of the sphere $S_n(r)$ with radius r. Then one counts the number $M_n(r)$ of points of the three-dimensional histogram contained inside the sphere $S_n(r)$; these are the points in the RGB space whose Euclidean distance to P_n is $\leqslant r$ (with no self-count, i.e. P_n itself is not included into the count M_n). The numbers $M_n(r)$ are then averaged over all the feasible centers P_n to yield the average count $M(r)$. In this process, to avoid border effects, only those centers P_n for which the sphere $S_n(r)$ is completely inside the cube $[0, Q-1]^3$ are considered as feasible centers to be taken into account in the averaging. $M(r)$ therefore represents the average number of neighbors within a distance r from a point of the three-dimensional histogram in the RGB space. The whole process is repeated as r is varied.

If the points of the three-dimensional histogram are uniformly scattered over the colorimetric space, with the constant density ρ, then one expects $M(r) = \rho 4\pi r^3/3$, i.e. $M(r) \propto r^D$ with $D = 3$, for points uniformly filling the three-dimensional space. Fractal sets of points are characterized by $M(r) \propto r^D$ with a generally noninteger fractal dimension D differing from 3. The power law $M(r) \propto r^D$ in itself is associated with scale invariance: when the scale in r is changed as $r \to \alpha r$, a corresponding change of scale in M as $M \to \alpha^D M$ makes the whole structure look similar. There is no underlying characteristic length in the structure, which is self-similar across scales. Uniform space filling with $D = 3$ is a trivial form of self-similarity. A noninteger exponent $D \neq 3$ in the power law, characterizes a nontrivial form of self-similarity, associated with a highly nonuniform, yet self-similar, way of filling the space. The points tend to aggregate in clusters of all sizes, separated by voids also of all sizes, in a self-similar way. There is no typical size for the clusters or for the voids. This type of fractal organization is observed for instance for the distribution of stars and galaxies [26], with a fractal dimension $D \approx 1.3$. It is also observed for percolation clusters, diffusion-limited aggregation processes, porous media, and other complex structures from many areas of natural sciences [26–29]. We are going to show that this type of fractal organization is also observed for the distribution of colors in the colorimetric space of natural images.

Another estimator for the correlation integral has been recently used in [30]. The estimator of [30] directly counts the number of pairs of pixels separated by a distance r in the histogram. This estimator of [30] is simpler to implement but it is sensitive to border effects at the boundaries of the colorimetric cube. As a consequence, it cannot be directly compared to available theoretical predictions for known distributions of points (for instance, uniform distributions at integer D as considered above). By contrast, the present estimator we shall use for the correlation integral avoids the border effects and can be directly compared to theoretical predictions on known distributions of points. This estimator will be applied here to corroborate the early results of [30], and to complement and extend the characterization of the fractal properties that may exist in the colorimetric organization of natural color images, this still standing as a novel topic for investigation.

3. Random test images

RGB color images with size 256×256 pixels, have been tested through the computation of their correlation integral $M(r)$ as defined above. To calibrate the approach, random color images synthesized with known statistical properties have been

tested first. A random image $\boldsymbol{I}_u(x_1,x_2)$ is generated in the following way. At each pixel (x_1,x_2), the value of each color component R, G and B, is picked at random in $[0,255=Q-1]$ with uniform probability. As a result, the pixels of such a random image $\boldsymbol{I}_u(x_1,x_2)$ uniformly distribute among the Q^3 colorimetric cells of the three-dimensional histogram, leading to an average number of neighbors $M(r)\propto r^D$ with $D=3$. This is precisely verified by the experimental count of $M(r)$ presented in Fig. 1. The log–log plot of Fig. 1 matching a straight line with slope 3, clearly reveals the expected power-law evolution $M(r)\propto r^3$. Only at very short distance $r\approx 1$, a small deviation exists in Fig. 1, which is explained as follows. In continuous space the volume of the sphere of radius $r=1$ is $4\pi/3\approx 4.2$, while on the discrete grid of the colors the number of discrete points within this sphere is 7. There is a much better match as soon as $r=2$, with a volume of the sphere of $4\pi 2^3/3\approx 33.5$ which comes very close to the number 33 of discrete points within the sphere. In Fig. 1, the small deviation at $r=1$ between the experimental count of $M(r)$ and the theoretical prediction $M(r)=\rho 4\pi r^3/3$, is precisely due to this difference between the volume of the sphere and the number of discrete grid points it contains. This deviation becomes rapidly negligible as r increases above 1, as visible in Fig. 1.

A second random image $\boldsymbol{I}_g(x_1,x_2)$ is generated with, at each pixel (x_1,x_2), the value of each component R, G and B selected independently with a Gaussian probability distribution with mean 128 and standard deviation 256/6, and then clipped into [0,255]. The resulting Gaussian random image $\boldsymbol{I}_g(x_1,x_2)$ is visible in Fig. 2. Random image $\boldsymbol{I}_g(x_1,x_2)$ is also characterized by a compact distribution of the colors in the colorimetric cube $[0,255]^3$, associated with a correlation integral $M(r)\propto r^D$ with $D=3$, as shown by the log–log plot of Fig. 3 closely matching a straight line with slope 3. In Fig. 3, a small deviation of $M(r)$ from the straight line is observed at short distance $r\approx 1$ where the count on discrete grid points may influence. And also in Fig. 3, a small deviation of $M(r)$ from the straight line is observed at large distance $r\approx 127$ because, due to their Gaussian distribution, colors become very rare at large distance, and the average number of neighbors $M(r)$ tends to cease to grow at large r in a finite realization. The similar behavior $M(r)\propto r^3$ for the random images $\boldsymbol{I}_u(x_1,x_2)$ and $\boldsymbol{I}_g(x_1,x_2)$ of Figs. 1 and 3, characterizes colors that are densely and evenly distributed in the colorimetric space.

A third test image $\boldsymbol{I}_f(x_1,x_2)$ is obtained by low-pass filtering of image $\boldsymbol{I}_g(x_1,x_2)$ in the following way: on $\boldsymbol{I}_g(x_1,x_2)$, the discrete cosine transform is taken for each image plane R, G and B. In each discrete cosine transform, with its frequency contents defined over $[0,255]\times[0,255]$, only the low-frequency contents in the domain $[0,10]\times[0,10]$ is kept, while the other (high)

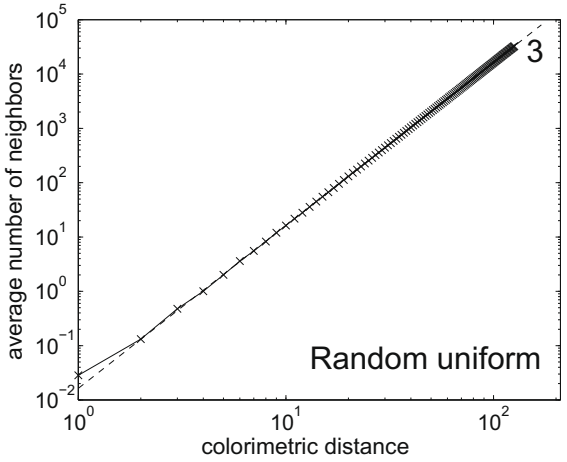

Fig. 1. For random image $\boldsymbol{I}_u(x_1,x_2)$, as a function of the colorimetric distance r, average number of neighbors $M(r)$ inside the sphere of radius r. The dashed line with slope 3 is the theoretical prediction $M(r)=\rho 4\pi r^3/3$ with $\rho=1/256$.

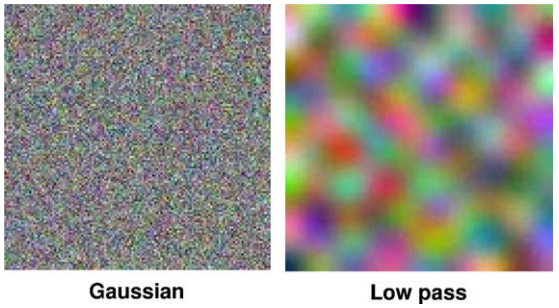

Fig. 2. Two random RGB color images with size 256×256 pixels and $Q=256$ levels: Gaussian $\boldsymbol{I}_g(x_1,x_2)$ (left), low pass $\boldsymbol{I}_f(x_1,x_2)$ (right). Both images have similar Gaussian independent R, G and B components, with no spatial dependence for $\boldsymbol{I}_g(x_1,x_2)$ (left), and with spatial correlation over around 25 pixels in length for $\boldsymbol{I}_f(x_1,x_2)$ (right).

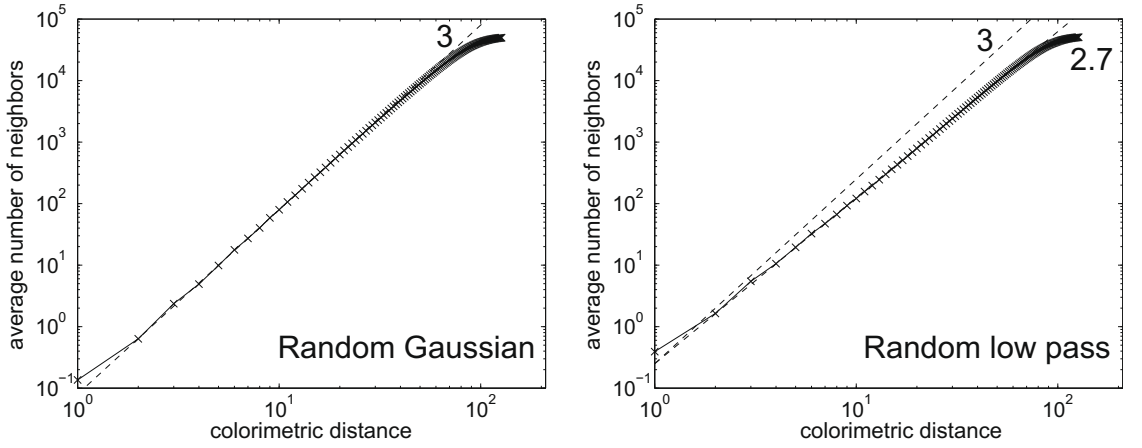

Fig. 3. As a function of the colorimetric distance r, average number of neighbors $M(r)$ inside the sphere of radius r, for the Gaussian random image $\boldsymbol{I}_g(x_1,x_2)$ (left) and for the low-pass random image $\boldsymbol{I}_f(x_1,x_2)$ (right) from Fig. 2. Dotted lines show the slopes 3 and 2.7.

frequency components are set to zero. Inverse cosine transform of each low-pass filtered plane R, G and B leads to image $\boldsymbol{I}_f(x_1,x_2)$. This linear filtering essentially preserves the Gaussian distribution of each independent components R, G and B for image $\boldsymbol{I}_f(x_1,x_2)$. However, spatial correlation is induced in each independent plane R, G and B of $\boldsymbol{I}_f(x_1,x_2)$, over around 25 pixels in length, in place of the independent pixel values in initial image $\boldsymbol{I}_g(x_1,x_2)$. Such a low-pass linear filtering is a simple way of generating spatially correlated structures of controlled size in the random image $\boldsymbol{I}_f(x_1,x_2)$, while keeping almost unaffected the Gaussian distribution of each independent component R, G and B. The resulting random image $\boldsymbol{I}_f(x_1,x_2)$ is visible in Fig. 2.

For random image $\boldsymbol{I}_f(x_1,x_2)$ with spatial correlation over each color plane R, G and B, the correlation integral $M(r)$ is presented in Fig. 3. As visible in Fig. 3, the log–log plot of $M(r)$ is closely matched by a straight line with slope 2.7. This is true except at short $r\approx 1$ and at large $r\approx 127$ where border effects similar to those already reported for Fig. 3 can play a part. Fig. 3 suggests the power-law evolution $M(r)\propto r^D$ with $D=2.7$. This power law is the mark of a scale-invariant distribution of the colors in the colorimetric space, but here with a nontrivial exponent $D=2.7$, which is clearly distinguished from the more trivial exponent $D=3$ by the measurements of Figs. 1 and 3. This is a rather remarkable behavior, for simple random test images, the induction of spatial correlations preserves the scale invariance of the color organization measured by $M(r)\propto r^D$, but with a change in the characteristic exponent D. This type of behavior of the distribution of colors is even more remarkable when we turn to natural color images, as we shall see in the next section.

As another random test image, we have constructed an RGB image whose colors are distributed on a two-dimensional manifold (a surface) in the colorimetric cube $[0,255]^3$. For this image, the red $X_1(x_1,x_2)$ and green $X_2(x_1,x_2)$ components are random independent components uniformly distributed over [0,255]; an auxiliary variable is $Z=0.1+0.9(X_1/255)(X_2/255)$, and the blue component is $X_3(x_1,x_2)=255\times 3(1-Z)Z$, resulting in an RGB image with the color histogram depicted in Fig. 4(left). The corresponding correlation integral $M(r)$ is presented in Fig. 4(right). The log–log plot of $M(r)$ is closely matched by a straight line with slope 2, associated to $M(r)\propto r^D$ with $D=2$, in accordance with the histogram obeying the two-dimensional manifold.

In a similar way, we have constructed an RGB image whose colors are distributed on a one-dimensional manifold (a curve) in the colorimetric cube $[0,255]^3$. For this image, we draw $Z(x_1,x_2)$ as an auxiliary random component uniformly distributed over $[0,1]$; then the red component is $X_1(x_1,x_2)=255(0.1+0.8Z^{0.9})$, the green component is $X_2(x_1,x_2)=255[0.1+0.4(1+\sin(2\pi Z))]$, and the blue component is $X_3(x_1,x_2)=255(0.1+0.8Z^{1.1})$, resulting in an RGB image with a color histogram according to a one-dimensional nonplanar curve in the colorimetric cube $[0,255]^3$. The corresponding correlation integral $M(r)$ is also presented in Fig. 4(right). The log–log plot of $M(r)$ is closely matched by a straight line with slope 1, associated to $M(r)\propto r^D$ with $D=1$, in accordance with the histogram obeying the one-dimensional manifold.

The results of this section validate the ability of the measure of $M(r)$ to identify an intrinsic dimension D relevant for the different test images. We now apply this measure to natural images.

4. Natural RGB color images

We have considered various common RGB color images, with size 256×256 pixels and $Q=256$ levels, shown in Fig. 5. For each of the color images of Fig. 5, we have computed the correlation integral $M(r)$ presented in Fig. 6. Two typical color histograms for such images are depicted in Fig. 7.

The remarkable observation in Fig. 6, is that in general the log–log plot of $M(r)$ is well approximated by a straight line, expressing a power-law behavior $M(r)\propto r^D$ as a common feature verified by the color images. This characterizes a scale invariance, or fractal organization, shared by the distributions of colors in the colorimetric space of the images. At the same

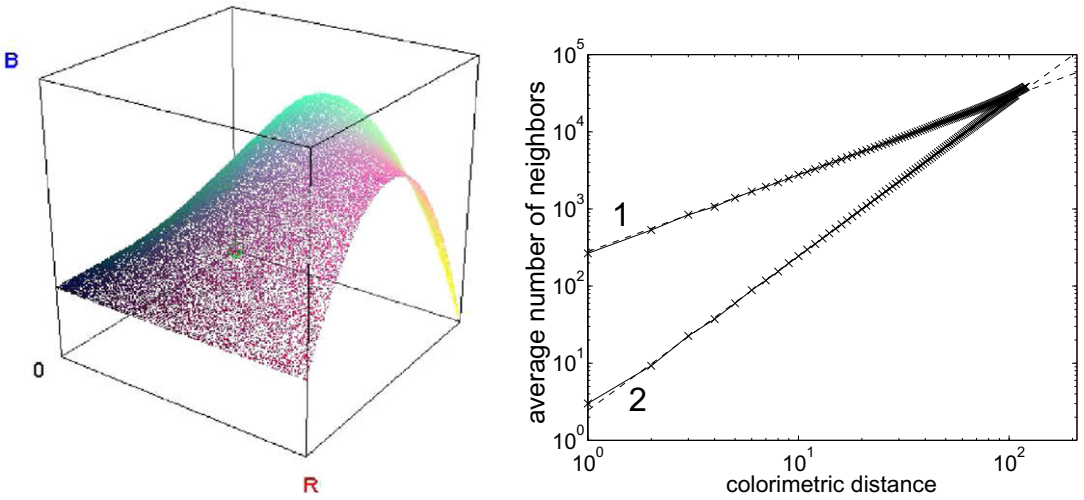

Fig. 4. A color histogram according to a two-dimensional manifold in the colorimetric cube $[0,255]^3$ (left); and (right): as a function of the colorimetric distance r, average number of neighbors $M(r)$ inside the sphere of radius r, for the histogram on the left around the slope 2, and for the histogram according to a one-dimensional manifold (see text) around the slope 1.

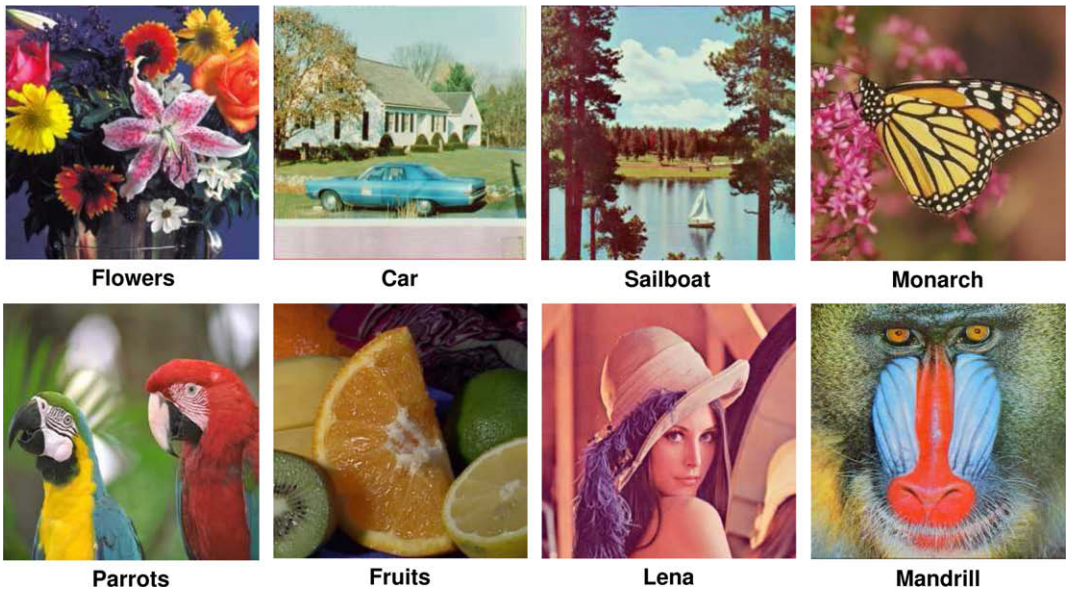

Fig. 5. Eight RGB color images with size 256×256 pixels and $Q = 256$ levels.

time in Fig. 6, the fractal exponent D takes significantly different nontrivial (noninteger) values among the color images, from $D = 1.3$ to $D = 2.3$ in Fig. 6. For the histogram of color images, Fig. 6 suggests a fractal organization with relevant features spanning many scales: clusters of colors spanning many sizes separated by voids with no colors also spanning many sizes, this in a self-similar way quantified by the fractal exponent D. In natural images, at small scales, clusters of very close colors reflect the many shades of a given reference color. At the other extreme, at large scales, the distribution is governed by the many significantly distinct colors usually composing a natural image as those of Fig. 5. Colorimetric structures may also exist at intermediate scales, as suggested by the uniform power-law behaviors of Fig. 6. The power law expresses this common scale-invariant fractal organization of the colors, and at the same time distinct values of the fractal exponent D clearly distinguish the various natural color images of Fig. 5. In this respect, image "Flowers" in Fig. 5 with $D = 1.3$ displays a value of fractal exponent for its color distribution similar to that of the distribution of stars and galaxies as given in [26].

5. Scaling invariance

The reduction of the number of colors of RGB images by rescaling and subquantization of their components, is a step commonly taken in image processing in order to decrease the complexity of subsequent operations. As a consequence of a self-

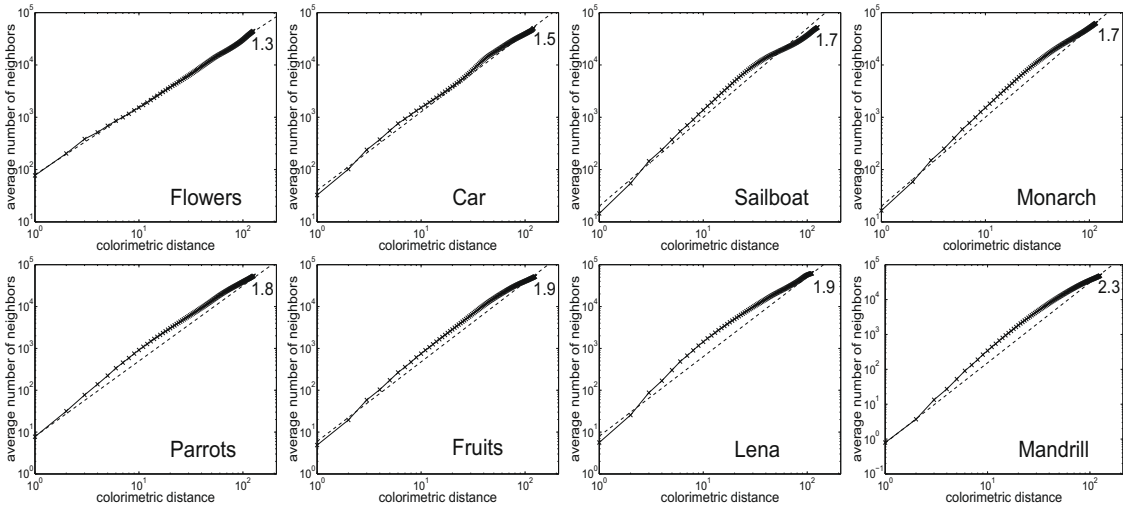

Fig. 6. As a function of the colorimetric distance r, average number of neighbors $M(r)$ inside the sphere of radius r, for the eight RGB color images of Fig. 5.

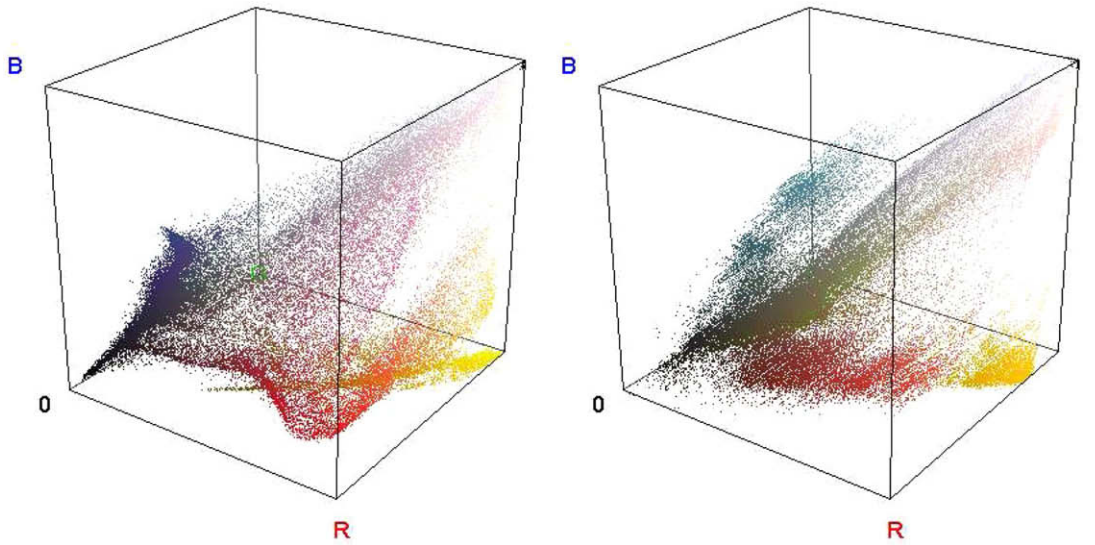

Fig. 7. Color histogram in the RGB colorimetric cube $[0,255]^3$ for image "Flowers" (left) and image "Parrots" (right) from Fig. 5.

similarity in the color organization, a scaling invariance should be observed in such a process of color reduction. We verify that the behavior of the correlation integral indeed manifests this expected scaling invariance. For an initial RGB color image, the number of colors is reduced by rescaling each initial color component $X_i \in [0,255]$ as $X_i \leftarrow \alpha X_i \in [0,255\alpha]$, with $0 < \alpha < 1$ and $i \in \{1,2,3\}$. The rescaled components are then quantized at integer values between 0 and 255α, and the correlation integral $M(r)$ is then computed in the reduced colorimetric cube $[0,255\alpha]^3$. Then the rescaled M obtained as $M \leftarrow \alpha^D M$ should precisely match the initial correlation integral prior to rescaling, as a consequence of the self-similarity. This is verified in Fig. 8.

For illustration in Fig. 8, we take $\alpha = (1/2)^{1/3}$, so as to reduce by a factor of $\alpha^3 = 2$ the overall number of possible colors in the image. We tested in Fig. 8 also $\alpha = (1/4)^{1/3}$, $(1/8)^{1/3}$ and $(1/16)^{1/3}$ reducing the number of possible colors, respectively, by 4, 8 and 16. In all cases the rescaled correlation integral superpose as visible in Fig. 8. This superposition is best at short distance in the colorimetric space, and gradually disrupts at large distance due to border effects. For instance when $\alpha = (1/4)^{1/3}$, when the overall number of possible color is divided by 4, each component X_i is rescaled from [0,255] into [0,161]. Therefore, border effects limiting the number of neighboring colors at large distance in the colorimetric space occur earlier after rescaling and color reduction. However, at short distance the power-law evolution is well preserved in the rescaling, as expected from the self-similarity of color organization.

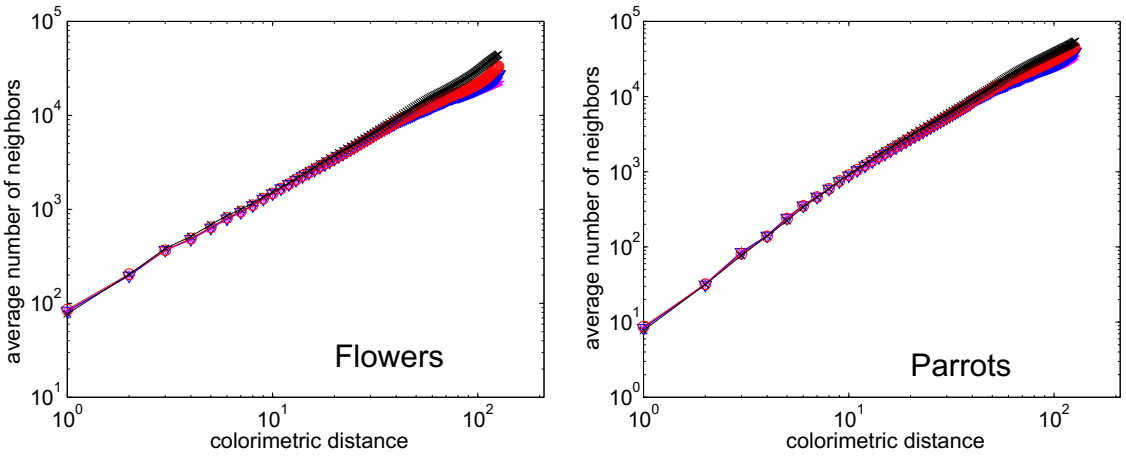

Fig. 8. Rescaled average number of neighbors $\alpha^D M$, as a function of the rescaled colorimetric distance αr, when rescaling the image components by $X_i \leftarrow \alpha X_i$. The condition $\alpha = 1$ ($\times$) corresponds to the original color image of Figs. 5,6, the three other conditions are $\alpha^3 = 1/2$ ($\circ$), $\alpha^3 = 1/3$ ($\triangledown$), $\alpha^3 = 1/4$ ($*$). The four curves superpose due to self-similarity of the color distribution. Images "Flowers" (left) and "Parrots" (right) from Fig. 5.

6. Other RGB images

Some natural color images have been found with a correlation integral $M(r)$ significantly departing from the power law $M(r) \propto r^D$. This has been observed to occur with natural images as those in Fig. 9 containing essentially a few dominant colors.

For the color images of Fig. 9, it appears in Fig. 10 that the average number of neighboring colors measured by $M(r)$ in the colorimetric space, tends to follow in log–log coordinates a concave ($\cap$) curve instead of a straight line. This can be explained as follows for natural images with a few dominant colors. Since the image is natural, a given color is modulated across many different shades. As a result, at short distance in the colorimetric space, there are many close neighboring colors, and consistently the average number of neighboring colors $M(r)$ tends to increase fast at short r. Also, since the image contains only a few significantly distinct colors, at large distance in the colorimetric space, there exists a relatively small number of neighboring colors. The average number of neighboring colors $M(r)$ therefore tends to increase slowly at large r. This is the characterization conveyed by the concave ($\cap$) shape in Fig. 10, for natural images with only a few dominant colors. This concave ($\cap$) departure is already slightly apparent for image "Lena" of Fig. 6, which tends to be dominated by a reddish-brownish tone. By contrast, natural images with a sufficient variety of colors were generally found to display a straight-line evolution for $M(r)$ in log–log coordinates, allowing to define the fractal exponent D.

7. Images with colormaps

For cost-effective image coding and communication, color images are often represented with a reduced number of colors under the form of indexed images associated to a colormap. The colormap keeps only a few colors that are well representative of the image, and it eliminates a huge number of colors originally possible in the RGB space. We want to examine how the self-similar color organization observed for RGB images is affected by the colormap representation. Different methods can be employed to construct a colormap suitable to an original RGB color image [31–33]. A common approach uses min-

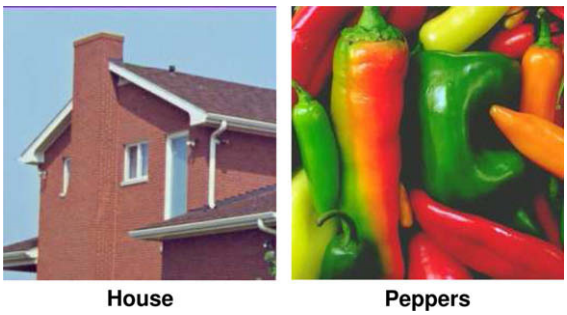

Fig. 9. Two RGB color images with size 256×256 pixels and $Q = 256$ levels.

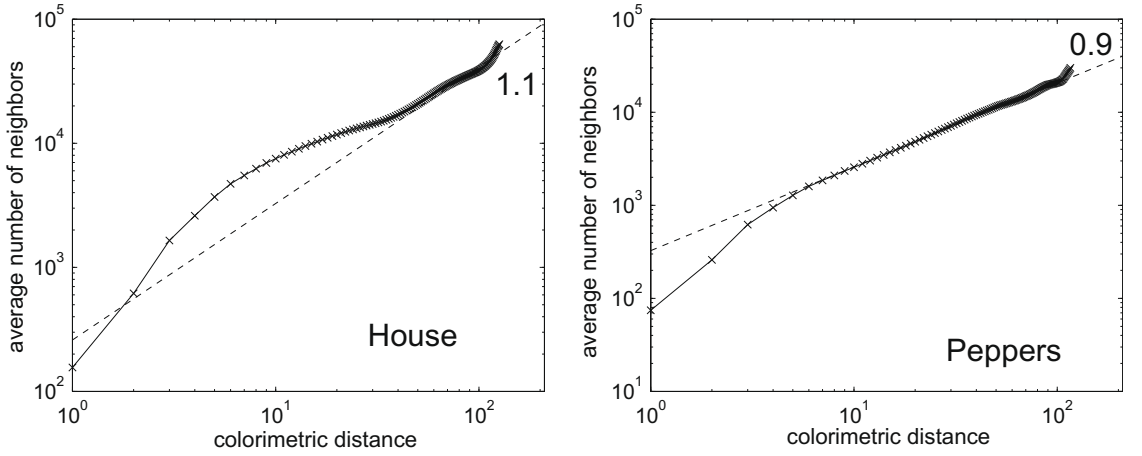

Fig. 10. As a function of the colorimetric distance r, average number of neighbors $M(r)$ inside the sphere of radius r: images "House" (left) and "Peppers" (right) from Fig. 9.

imum variance quantization, by which the number of colors in the colormap is first decided, and then each color of the colormap is selected as a centroid of the Voronoi partition of the three-dimensional histogram of the original RGB color image, the centroids and partition being iteratively stabilized through a clustering process like the K-means or the like [31]. We have studied the impact of such a colormap reduction of the number of colors on the correlation integral $M(r)$. Fig. 11 presents the evolution of $M(r)$ when RGB color images from Fig. 5 are coded with colormaps of different sizes.

Fig. 11 shows that the effect of coding the original colors by means of a reduced colormap, has a drastic effect on the power-law evolution of $M(r)$. In log–log coordinates in Fig. 11, the straight-line evolution of $M(r)$ characterizing the self-similar organization of the original colors, is replaced with colormaps by a convex ($\cup$) evolution of $M(r)$ with an horizontal plateau at short distance r. The reason is that the original colors that form a cluster of close neighboring colors are replaced by one common representative color in the colormap. As a result, in images with a colormap, the average number of neighboring colors does not increase at short distance, leading to an horizontal plateau at short r. Consistently, the extension of this horizontal plateau increases as the number of colors in the colormap diminishes, as visible in Fig. 11. Now at large distance, the evolution of $M(r)$ is governed by colors that are significantly separated in the colorimetric space. These well separated colors are adequately reproduced in the colormap. As a result, the evolution of $M(r)$ at large r, is essentially the same in the image with the colormap and in the original RGB image. Especially, the straight-line evolution with slope D is recovered at large r, as visible in Fig. 11.

Natural RGB color images as those of Fig. 5 have a rich colorimetric organization, with uniform self-similar distribution of the colors in the colorimetric space at all existing scales. Color reduction by colormaps breaks this uniform self-similarity, as it realizes a much poorer representation of the colorimetric variety at small scales in the colorimetric space.

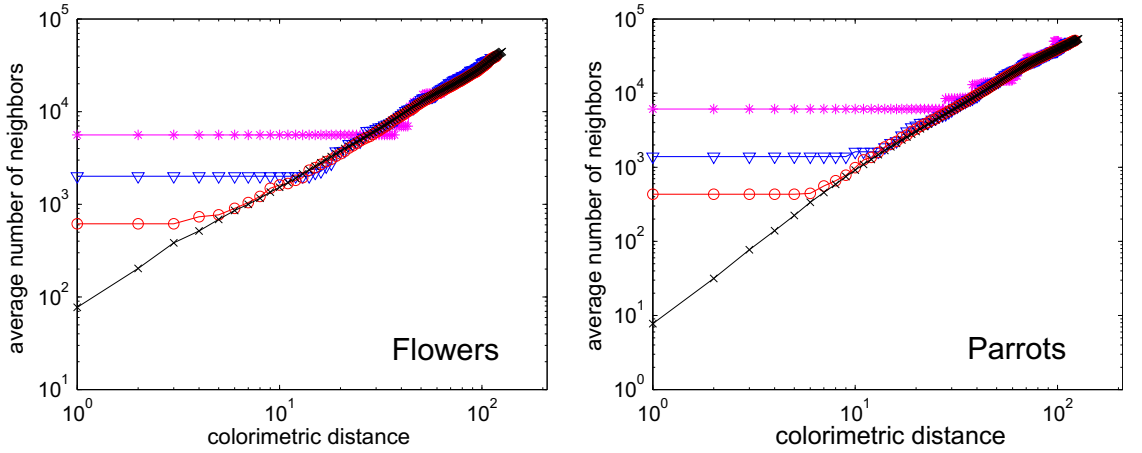

Fig. 11. As a function of the colorimetric distance r, average number of neighbors $M(r)$ inside the sphere of radius r. Original RGB image ($\times$), image reduced to a colormap of 256 colors ($\circ$), of 64 colors ($\triangledown$), of 16 colors ($*$): images "Flowers" (left) and "Parrots" (right) from Fig. 5.

The various possible evolutions of $M(r)$ provide a flexible characterization of the distribution of colors in the colorimetric space. Concave ($\cap$) evolutions of $M(r)$ as in Fig. 10 characterize color distributions that are rich at small scales and relatively poorer at large scales. On the contrary, convex ($\cup$) evolutions of $M(r)$ as in Fig. 11 characterize color distributions that are poor at small scales and richer at large scales. In-between, natural color images with sufficient variety of colors tend to display self-similar colorimetric distributions, uniformly organized over all existing scales.

8. Gray images

The fractal characterization in the RGB space can also be applied to gray images. Gray images with a single gray-level component $X(x_1, x_2)$ can be represented by three-component RGB images constrained to have three identical components $R = G = B = X(x_1, x_2)$. For such images, it is found that the characterization in the RGB space usually gives a correlation integral $M(r) \propto r^D$ with $D = 1$, as visible in Figs. 12 and 13.

Natural images typically lead to a broad distribution of gray giving way to a correlation integral $M(r) \propto r^D$ with $D = 1$. The fractal distribution of colors that may exist in natural color images, collapses into a one-dimensional distribution for gray images. While colors may fill the three-dimensional colorimetric space in a very irregular and fractal organization characterized by noninteger D, the gray levels fill the one-dimensional space available to them in a more regular and uniform way characterized by $D = 1$, as illustrated by Fig. 13.

9. Discussion

It is known that the three RGB color components of natural images are usually strongly correlated and dependent. The present study points to a fractal structure for these correlations and to self-similar dependences among the three components. This has been obtained by studying the correlation integral $M(r)$ for a characterization of the three-dimensional color histogram of RGB images. A remarkable observation is that $M(r)$, for natural images with sufficient colorimetric richness or variety, tends to follow a power-law form. This observation is remarkable in the sense that $M(r)$ could a priori be any nondecreasing function. Yet, power-law evolution of $M(r)$ seems to be a typical behavior for natural color images. Moreover, the exponent D of the power law $M(r) \propto r^D$ is usually found to be noninteger, with a value of D characteristic of a given natural image. These observations identify a fractal or multiscale self-similar organization of the colors found in typical natural images. We emphasize that the present fractal properties observed in the *colorimetric* organization of natural images are different from other fractal properties previously reported for natural images in their *spatial* organization [1,3,4,18,6]. Briefly stated, previous results [1,3,4,18,6] dealt with fractal distribution of the pixels in space, while the present results deal with fractal distribution of the pixels in the colorimetric cube. This is a novel point of view on fractal properties in images. In this respect, the current application of fractal concepts to image compression is more related to the spatial organization of images [34–37], while here fractality in the colorimetric organization of images opens up a new perspective.

Explanation for this fractal organization that tend to display the colors in natural images, can be proposed in two (possibly connected) directions. The fractal organization of the colors could be related to the properties of the natural scenes, which typically can contain many different structures and objects of various sizes and colors, appearing at various depths, various angles, under various lighting and shading conditions. These combined ingredients could lead to the existence in typical natural scenes, of many colors with each color affected by many modulating factors, these together building up a fractal organization for the colors. In this respect, the fractal structure in the color distribution would share some origin in common with other fractal properties found in the spatial organization of natural images, and stemming from multiscale features of natural scenes. In another direction, the fractal organization of the colors could be related to the coding properties of the visual system. Trichromacy, at the root, is essentially a coding modality of the visual system [38]. Given typical spectral statistics and properties of the light in our natural environment, the visual system may have evolved its coding capabilities towards a multiscale representation of the visible spectrum. At large scales are colors that are far apart in the visible spectrum. At small scales are colors that are close together, as for instance the gradation of shades of a given reference color. There are also

Fig. 12. Two gray-level images with size 256×256 pixels and $Q = 256$ levels, coded as RGB color images constrained by R = G = B.

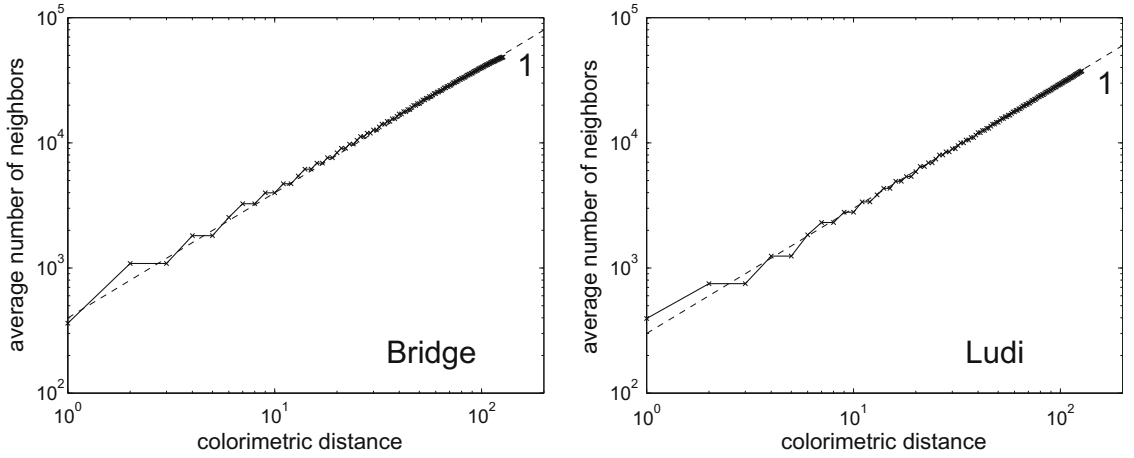

Fig. 13. As a function of the colorimetric distance r, average number of neighbors $M(r)$ inside the sphere of radius r, for the two gray-level images "Bridge" (left) and "Ludi" (right) from Fig. 12.

intermediate scales of colors, like for example all the different greens or browns that can exist in a forest or an outdoor landscape; and yet other scales. All these spectral scales can convey useful information for efficient interaction with the environment. For efficient processing and discrimination of these multiple scales, the visual system may have distributed its coding capabilities evenly over this whole range of scales of the color information. The fractal structure reported in this paper could be a manifestation of this coding organization in the visual system.

The present results concerning a fractal organization of colors remain to be confirmed and studied in more detail with extensive surveys of natural images. This would be useful to appreciate in more depth the conditions of validity of the power-law evolution $M(r) \propto r^D$ which seems to be rather common for natural images, and also to understand the origin of this behavior and of the different values observed for the fractal exponent D. Also, complementary methods other than the correlation integral could be used to further characterize fractal properties in the color organization. Similar fractal characterization could also be examined for the analysis of multispectral images with more than three components [39].

The present results may provide a useful parameter, with the fractal exponent D, for a concise characterization of the complex organization of a color image in its colorimetric space. This could serve for instance to image recognition, classification and indexing. The results may also bear significance for image segmentation from the color histogram. If a fractal structure applies for the histogram, this means that there tend to exist clusters of colors of many sizes spanning many scales in the colorimetric space. This would be so instead of a few dominant and well delineated clusters of colors. In a segmentation process, if one looks for peaks of the color histogram to define classes, one may have to cope with many peaks at different scales (peaks with subpeaks and subsubpeaks over many scales, in a self-similar way), according to the fractal dimension D. The reported results could also allow more accurate modeling of natural images. Multiscale and fractal properties, as observed experimentally in natural images, are been recognized as important cues for developing efficient image models [11–15]. Such approach has been undertaken essentially for gray-level images, and it could be extended to color images based on the observations we report here. The present results may also have value for image synthesis, to construct color palettes with the realism conferred by a fractal structure as observed in natural images. Finally, as we mentioned earlier, investigation of possible fractal structures and properties in natural images, may provide a path to contribute to better understanding of the coding and processing abilities of the visual system, and lead to progress in computer vision.

Acknowledgement

Julien CHAUVEAU acknowledges support from *La Communauté d'Agglomération du Choletais*, France.

References

[1] Burton GJ, Moorhead IR. Color and spatial structure in natural scenes. Appl Opt 1987;26:157–70.
[2] Field DJ. Relation between the statistics of natural images and the response properties of cortical cells. J Opt Soc Am A 1987;4:2379–94.
[3] Ruderman DL, Bialek W. Statistics of natural images: scaling in the woods. Phys Rev Lett 1994;73:814–7.
[4] Ruderman DL. Origins of scaling in natural images. Vision Res 1997;37:3385–98.
[5] Field DJ. What is the goal of sensory coding? Neural Comput 1994;6:559–601.
[6] Hsiao WH, Millane RP. Effects of occlusion, edges, and scaling on the power spectra of natural images. J Opt Soc Am A 2005;22:1789–97.
[7] Dong DW, Atick JJ. Statistics of natural time-varying images. Network: Comput Neural Syst 1995;6:345–58.
[8] Ruderman DL. The statistics of natural images. Network: Comput Neural Syst 1994;5:517–48.
[9] Olshausen BA, Field DJ. Vision and the coding of natural images. Am Sci 2000;88:238–45.
[10] Geisler WS. Visual perception and the statistical properties of natural scenes. Ann Rev Psychol 2008;59:167–92.

[11] Lee AB, Mumford D, Huang J. Occlusion models for natural images: a statistical study of a scale-invariant dead leaves model. Int J Comput Vision 2001;41:35–59.
[12] Srivastava A, Liu X, Grenander U. Universal analytical forms for modeling image probabilities. IEEE Trans Pattern Anal Mach Intell 2002;24:1200–14.
[13] Srivastava A, Lee AB, Simoncelli EP, Zhu SC. On advances in statistical modeling of natural images. J Math Imaging Vis 2003;18:17–33.
[14] Gousseau Y, Roueff F. Modeling occlusion and scaling in natural images. SIAM J Multiscale Model Simulat 2007;6:105–34.
[15] Chainais P. Infinitely divisible cascades to model the statistics of natural images. IEEE Trans Pattern Anal Mach Intell 2007;29:2105–19.
[16] Webster MA, Mollon JD. Adaptation and the color statistics of natural images. Vision Res 1997;37:3283–98.
[17] Párraga CA, Brelstaff G, Troscianko T, Moorehead IR. Color and luminance information in natural scenes. J Opt Soc Am A 1998;15:563–9.
[18] Turiel A, Parga N, Ruderman DL, Cronin TW. Multiscaling and information content of natural color images. Phys Rev E 2000;62:1138–48.
[19] Gevers T, Smeulders AWM. Color-based object recognition. Pattern Recogn 1999;32:453–64.
[20] Syeda-Mahmood T, Petkovic D. On describing color and shape information in images. Signal Process: Image Commun 2000;16:15–31.
[21] Batlle J, Casalsb A, Freixeneta J, Martía J. A review on strategies for recognizing natural objects in colour images of outdoor scenes. Image Vision Comput 2000;18:515–30.
[22] Cheng YC, Chen SY. Image classification using color, texture and regions. Image Vision Comput 2003;21:759–76.
[23] Peitgen HO, Saupe D, editors. The science of fractal images. Berlin: Springer; 1988.
[24] Turner MJ, Andrews PR, Blackledge JM. Fractal geometry in digital imaging. New York: Academic Press; 1998.
[25] Mao X, Chen B, Muta I. Affective property of image and fractal dimension. Chaos, Solitons & Fractals 2003;15:905–10.
[26] Mandelbrot BB. The fractal geometry of nature. San Francisco: Freeman; 1983.
[27] Gouyet JF. Physics and fractal structures. Berlin: Springer; 1996.
[28] Havlin S, Buldyrev SV, Goldberger AL, Mantegna RN, Ossadnik SM, Peng CK, et al. Fractals in biology and medicine. Chaos, Solitons & Fractals 1995;6:171–201.
[29] El Naschie MS. The impact of nonlinear dynamics and fractals on quantum physics and relativity. Chaos, Solitons & Fractals 1998;9:1009–10.
[30] Chauveau J, Rousseau D, Chapeau-Blondeau F. Pair correlation integral for fractal characterization of three-dimensional histograms from color images. Lecture notes in computer science, LNCS 5099. Berlin: Springer; 2008. pp. 200–208.
[31] Sharma G, editor. Digital color imaging handbook. Boca Raton (FL): CRC Press; 2003.
[32] Orchard MT, Bouman CA. Color quantization of images. IEEE Trans Signal Process 1991;39:2677–90.
[33] Braquelaire JP, Brun L. Comparison and optimization of methods of color image quantization. IEEE Trans Image Process 1997;6:1048–52.
[34] Jacquin AE. Image coding based on a fractal theory of iterated contractive image transformation. IEEE Trans Image Process 1992;1:18–30.
[35] Fisher Y. Fractal image compression: theory and applications. Berlin: Springer; 1995.
[36] Truong TK, Kung CM, Jeng JH, Hsieh ML. Fast fractal image compression using spatial correlation. Chaos, Solitons & Fractals 2004;22:1071–6.
[37] Wu MS, Teng WC, Jeng JH, Hsieh JG. Spatial correlation genetic algorithm for fractal image compression. Chaos, Solitons & Fractals 2006;28:497–510.
[38] Sharma G, Trussel HJ. Digital color imaging. IEEE Trans Image Process 1997;6:901–32.
[39] Landgrebe D. Hyperspectral image data analysis. IEEE Signal Process Mag 2002;19(1):17–28.